

Penetration mechanism of cells by vertical nanostructuresJing Zou, Jinqi Li, Tongsheng Chen, and Xinlei Li ^{*}*MOE Key Laboratory of Laser Life Science & Institute of Laser Life Science, College of Biophotonics,
South China Normal University, Guangzhou 510631, China
and Guangdong Provincial Key Laboratory of Laser Life Science, College of Biophotonics,
South China Normal University, Guangzhou 510631, China* (Received 22 July 2020; revised 26 September 2020; accepted 21 October 2020; published 4 November 2020)

Cell penetration by high aspect-ratio vertical nanostructures such as nanowires and nanopillars provides a powerful method for accessing the cell interior for delivery and sensing. However, there is a lack of studies on the understanding of the mechanism of cell membrane penetration and how design nanostructures to optimize the efficiency of penetration remains unclear. Here, we propose an analytical model to elucidate the mechanism of cells penetration by analyzing the free-energy change of cells adhered to the nanostructures surface. Furthermore, we provide a simple method to evaluate the crossover radius or density for cell membrane penetration. By introducing a dimensionless parameter, i.e., adhesion area factor, we investigated the effects of the radius and distribution densities of nanostructures on cell membrane penetration which is determined by the competition between adhesion energy and deformation energy. Besides, a diagram of the distribution of cell penetration and no penetration is obtained. From the cell penetration diagram, one can determine easily and intuitively the relations of cell penetration state with the radius and distribution densities of nanostructures. Our theoretical results seem to show broad agreement with experimental observations, which implies that these studies would provide useful guidance to the design of nanopatterned surfaces for biomedical applications.

DOI: [10.1103/PhysRevE.102.052401](https://doi.org/10.1103/PhysRevE.102.052401)**I. INTRODUCTION**

Arrays of nanostructures have become one of the branches of advantageous tools that promote the interaction of cells with substrate, and have been used for specific cell capture [1–4], intracellular delivery (detection) [5–8], cellular activity regulation [9–11]. In recent years, the researchers found that vertical nanostructures such as nanowires and nanopillars with small radius or low density can penetrate into the cell. The penetration of the cell by nanostructures provides a method to gene transfection and drug delivery [12–17]. The gene transfection and delivery of drugs by cell penetration have some distinct advantages over other methods including endocytosis and electroporation. Cell penetration not only has a high efficiency of transfection and delivery, but also does almost no harm to cells because the pores induced by penetration have the size of only several tens of nanometers [18–22]. The experimental results show that cells can only be penetrated by the nanostructures with particular size; in other words, the geometry of nanostructures strongly influences cell penetration [18,19,23–25]. In experiments, cells can be penetrated by the nanocones or nanopillars with small radius or low density, while the nanocones or nanopillars with large radius or high density cannot penetrate cells. Despite the growing interest and considerable recent progress in the cell penetration by nanostructures, so far the mechanisms of cell penetration it is still not well understood, and how design nanostructures optimize the efficiency of penetration remains unclear. There

is much to be learned about the specific mechanisms. For example, what geometry of nanostructures can penetrate cells? Which factors are related to cell penetration and how to influence cell penetration? In order to attempt to design and fabricate new and preferable artificial nanostructures surfaces to penetrate cell, quantitative theories have been requested to study the mechanisms of cell penetration.

In this work, we propose an analytical thermodynamic model to study the mechanism of cell membrane penetration by analyzing the free-energy change of cells adhered to the nanostructures surface. Our theoretical results reveal that the cell penetration is determined by the competition between deformation energy of membrane and the formation energy of pore caused by penetration. We provide a simple method to calculate the crossover radius or density of cell membrane penetration and no penetration. Furthermore, we construct a phase diagram to clarify the inter-related effects of the radius and surface distribution density on the cell penetration.

II. THEORETICAL MODEL

An array of nanostructure is adopted in our calculated model, as shown in Fig. 1. According to the experimental observations, the cell membrane can extend into the gap among the nanostructures and tightly adheres to the side walls of the nanostructures when the cell adheres to the nanostructure array. During the adhesion process, the cell membrane suffers from a large amount of deformation. When the deformation of membrane exceeds a certain degree, the cell membrane would split and be penetrated by the nanostructures, as the experimental results display [20–22,26,27]. Therefore, it is

^{*}xlli@snu.edu.cn

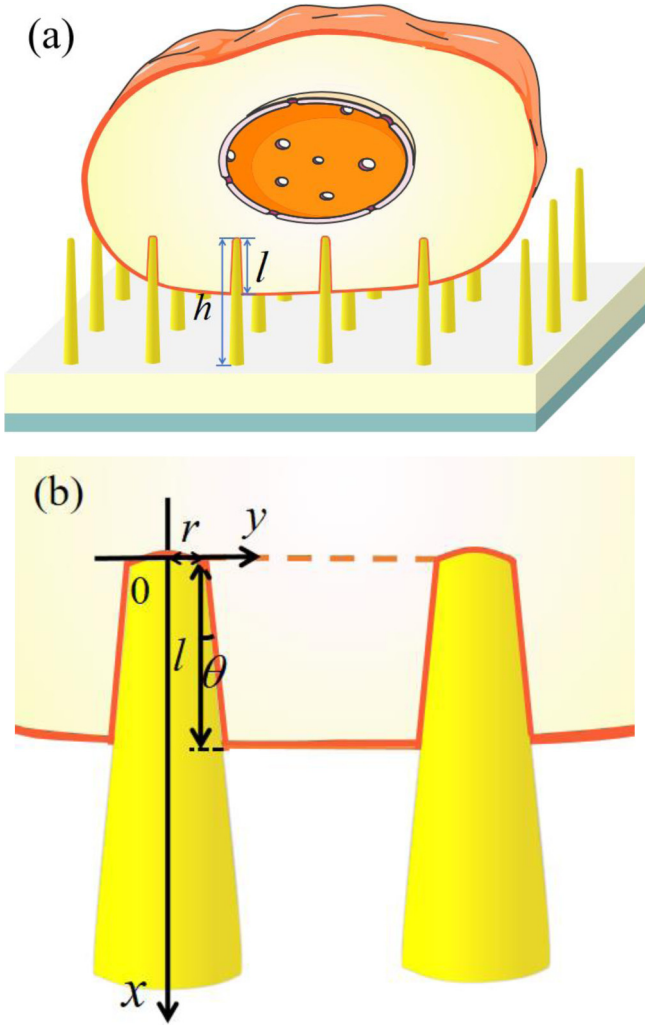


FIG. 1. (a) Schematic illustration of the cell adhered to truncated nanocone array. (b) The enlarged views of the membrane adhered to the truncated nanocone array in (a).

important for penetrating the cell membrane to study the deformation of membrane during adhesion process. The deformation of the cell membrane is mainly determined by the following two aspects, one is bending deformation caused by the changes of the surface curvature of membrane [28], and the other is stretching deformation caused by the increase of cell membrane area. Considering the effects of the bending energy and stretching energy, the total deformation energy can be written as

$$E_{\text{def}} = \int_{S_b} \left[\frac{\kappa}{2} (c_1 + c_2 - c_0)^2 \right] dS + \frac{1}{2} \lambda \frac{\Delta S^2}{S_0}, \quad (1)$$

where κ is the bending modulus of the membrane, c_1 (c_2) and c_0 denote the principal curvatures of the bending membrane surface, and the spontaneous curvature, respectively, S_b is the intracellular bending area. λ denotes the stretching modulus of the membrane, ΔS and S_0 denote the intracellular area change by stretching and the cell area before stretching, respectively. The first term is bending energy, and the second term represents stretching energy.

A. Truncated nanocone array

As a typical nanostructure, truncated nanocone arrays were usually used to penetrate cells for gene transfection and drug delivery [18,25,29]. In our model, we assume that the truncated nanocones are located at the sites of an ideal square lattice with a surface distribution density of ρ (the number of nanocones per unit area), the angle between the side of the truncated nanocones and the vertical direction is θ , and the radius of the top is r , as shown in Fig. 1(b). When the cell initially adheres to the truncated nanocones, the cell membrane does not exhibit bending and stretching changes, so the deformation of the cell membrane is initially equal to zero. During the following adhesion process, the membrane extends into the space of nanostructures and adheres to the side wall of the nanostructures, accompanying bending deformation and stretching deformation. The surface principal curvature of the truncated nanocones is $c_1 = 0$, and $c_2 = \cos \theta / (r + x \tan \theta)$, where x is the distance from the top surface to the local point [establish the coordinate system as shown in Fig. 1(b)]. If we select a period square domain as a study object, when the adhesion depth is l , the bending-energy change of the cell membrane can be written as

$$E_{\text{Bend}} = \int_0^l \frac{\kappa}{2} \left(\frac{\cos \theta}{r + x \tan \theta} \right)^2 2\pi (r + x \tan \theta) d \left(\frac{x}{\cos \theta} \right). \quad (2)$$

When $\theta > 0$,

$$E_{\text{Bend}} = \pi \kappa \frac{\cos^2 \theta}{\sin \theta} \ln \frac{r + l \tan \theta}{r}. \quad (3)$$

The cell membrane area in our selected period square domain before stretching, S_0 , is equal to $1/\rho$. When cell adhesion occurs, the cell membrane can stretch and adhere to its side walls. In this case, the area of the cell membrane becomes $S = S_0 + S_{\text{ad}} + \pi r^2 - \pi (r + l \tan \theta)^2$, where S_{ad} denotes the adhesion area that $S_{\text{ad}} = \pi l (2r + l \tan \theta) / \cos \theta$. So the change of membrane area is $\Delta S = S - S_0$. The stretching energy of the cell membrane can be calculated by

$$E_{\text{str}} = \frac{\lambda}{2} \frac{[\pi (2r + l \tan \theta) \frac{l}{\cos \theta} - \pi (r + l \tan \theta)^2 + \pi r^2]^2}{1/\rho}. \quad (4)$$

Considering the contribution of adhesion energy, the total free energy is that

$$E = -\gamma S_{\text{ad}} + E_{\text{Bend}} + E_{\text{str}}, \quad (5)$$

where γ is the adhesion energy per unit area between the cell membrane and the surface; three energies are considered: bending energy, stretching energy, and adhesion energy in this paper [30]. According to the principle of minimum energy, the cell membrane is in the lowest-energy state (steady state) and further adhesion is unfavorable when the adhesion depth reaches a critical value. From $\partial E / \partial l = 0$, one can derive the critical adhesive depth at the steady state, l^* , as (detailed calculations can be found in Appendix A):

$$l^* = [\sqrt{(\sqrt{b^2 - 4ac} - b)/2a} - r] / \tan \theta, \quad (6)$$

where $a = 2\pi^2 \lambda \rho \tan \theta (1/\sin \theta - 1)^2$, $b = -(ar^2 + 2\gamma\pi / \cos \theta)$, $c = \pi \kappa \cos \theta$.

When the cell is penetrated by the nanostructures, the truncated nanocones should move apart the lipids of membrane and create a pore with at least radius of r . Therefore, the formation of the pore must overcome an energy barrier, i.e., pore formation energy. The pore formation energy is due to breaking the contacts between phospholipids lying on membrane close to the edge of the pore, which is proportional to the perimeter of the pore. If we set the line density of pore formation energy as e , the energy barrier required for the cell membrane to be penetrated is $2\pi r e$. During the process of cell adhesion, the cell membrane suffers comparatively large deformation. The deformation can result in the breakdown of bonding between phospholipids lying on membrane if the deformation exceeds a critical degree. In other words, when the deformation energy of the membrane is larger than the pore formation energy, the cell membrane can be penetrated by the nanostructures. Therefore, we can determine cell membrane penetration by comparing the deformation energy and the pore formation energy. Because the deformation energy increases with the increase of the adhesion depth, we can compare the critical deformation energy E_{def}^* at the steady state ($l = l^*$) and the pore formation energy to judge whether the cell membrane is penetrated. This discriminant formula can be written as

$$\Delta E^* = \pi \kappa \frac{\cos^2 \theta}{\sin \theta} \ln \frac{r + l^* \tan \theta}{r} + \frac{\lambda \rho}{2} \times \left[\frac{\pi l^*}{\cos \theta} (2r + l^* \tan \theta) + \pi r^2 - \pi (r + l^* \tan \theta)^2 \right]^2 - 2\pi r e. \quad (7)$$

If $\Delta E^* > 0$, it means that the deformation energy is greater than pore formation energy, and the cell membrane will be penetrated before achieving steady state. In this case, the formation of cell membrane pore can effectively reduce the deformation energy stored in the membrane by reducing the membrane area and bending at the position of membrane pore. In detail, when the pore forms, the membrane area decreases, and the corresponding stretching energy is released. In addition, because the top of the nanopillars has the maximum surface curvature (that is, the maximum bending energy), the bending energy can be reduced by the most when the pore forms at the position. By contrast, the cell membrane will not be penetrated if $\Delta E^* < 0$.

B. Vertical nanopillars array

As special truncated nanocones ($\theta = 0^\circ$), vertical nanopillars array can also be used to penetrate the cell membrane [30]. In this case, $S_{ad} = 2\pi r l$, and $\Delta S = S_{ad} = 2\pi r l$. Therefore, the total energy can be calculated by a simple expression that $E = -2\gamma\pi r l + \kappa\pi l/r + 2\lambda\rho(\pi r l)^2$. Using $\partial E/\partial l = 0$, we can derive the critical adhesive depth l^* as

$$l^* = \frac{2\gamma r^2 - \kappa}{4\lambda\rho\pi r^3} \quad (8)$$

Similarly, the formula for determining whether the cell membrane can be penetrated by vertical nanopillars becomes

$$\Delta E^* = \frac{\kappa\pi l^*}{r} + 2\lambda\rho(\pi r l^*)^2 - 2\pi r e. \quad (9)$$

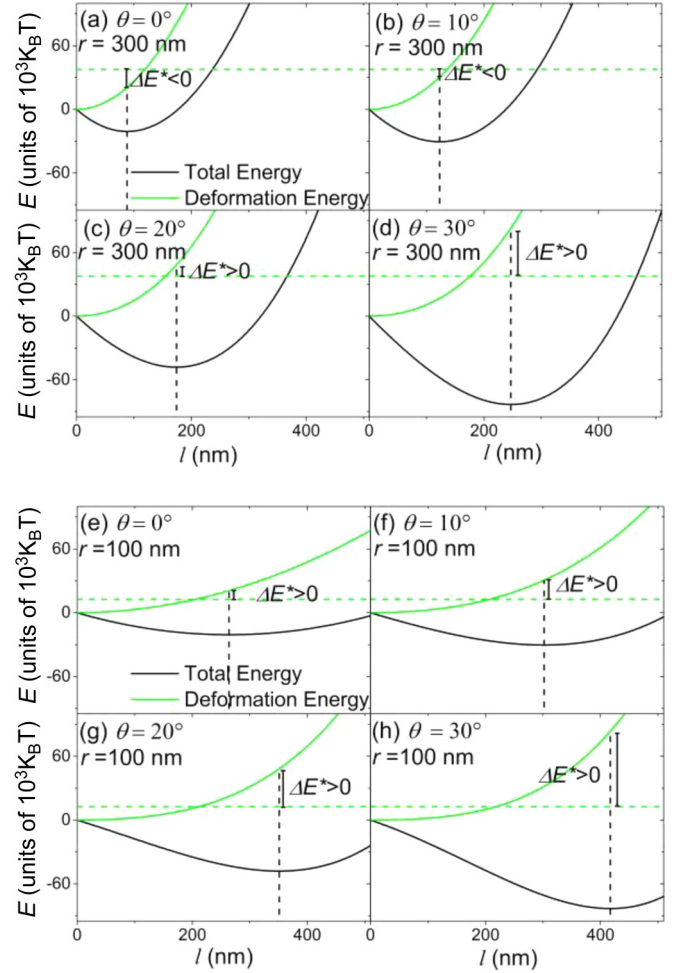


FIG. 2. The calculated free energy and deformation energy as functions of adhesion depth of cell membrane adhered to truncated nanocone array surface with different tilted angle (a) $\theta = 0^\circ$, (b) $\theta = 10^\circ$, (c) $\theta = 20^\circ$, (d) $\theta = 30^\circ$ when $\rho = 0.3 \mu\text{m}^{-2}$, $r = 300$ nm, (e) $\theta = 0^\circ$, (f) $\theta = 10^\circ$, (g) $\theta = 20^\circ$, (h) $\theta = 30^\circ$ when $\rho = 0.3 \mu\text{m}^{-2}$, $r = 100$ nm. The pore formation energy is indicated by a green dotted line.

III. RESULTS AND DISCUSSION

Based on the established model above, we can study the mechanism of cell penetration through analyzing total free energy, deformation energy, and pore formation energy. Figure 2 depicts the calculated energies as the function of the adhesion depth under different θ and r , when $\rho = 0.3 \mu\text{m}^{-2}$ (30 per $100 \mu\text{m}^2$). In our calculations, the related parameters are $\gamma = 0.25 k_B T/\text{nm}^2$ [6,31,32], $\kappa = 20 k_B T$ [31], $\sigma = 0.3 k_B T/\text{nm}^2$, and $\lambda = 5 k_B T/\text{nm}^2$ [33]. We can find that the total free energy firstly decreases and then increases with increasing adhesion depth, which means that there is a steady state which corresponds to the minimum of total energy when $l = l^*$, as shown by the black solid line in Fig. 2. However, the deformation energy of cell membrane increases with increasing adhesion depth and achieves maximum when $l = l^*$ (the green solid line in Fig. 2). The pore formation energy is relative to the size of the pore. So, the pore formation energy is a constant when the radius of nanostructures is fixed, as

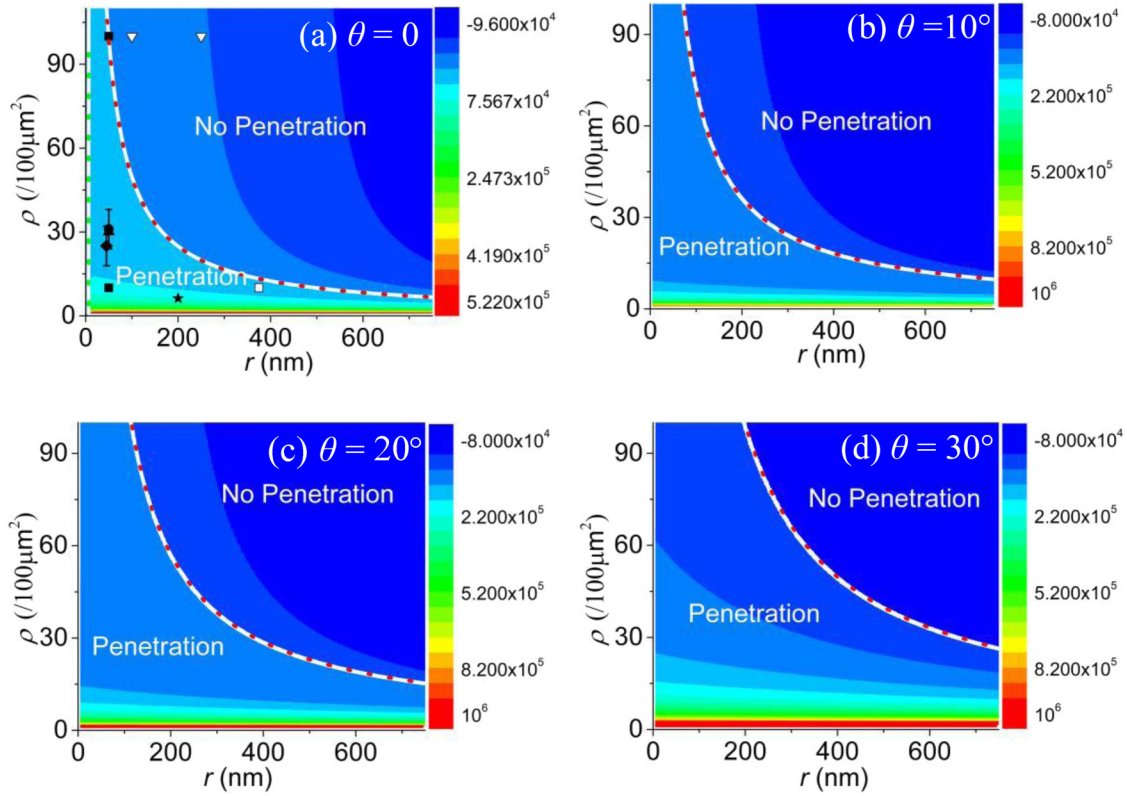


FIG. 3. The cell penetration diagram in the space of the $r - \rho$ plane under infinite long truncated nanocones with different tilted angle (a) $\theta = 0^\circ$, (b) $\theta = 10^\circ$, (c) $\theta = 20^\circ$, and (d) $\theta = 30^\circ$, respectively. The color bar indicates the calculated values of the difference between the deformation energy and the pore formation energy, ΔE^* , based on Eq. (7). The white line divide cell state into two modes, “penetration” and “no-penetration” mode, according to whether the value of ΔE^* is greater than zero. The red dotted line is calculated according to Eq. (10) or (11). In (a), the various solid points correspond to experimental data for the cell membrane penetration, and the various hollow points correspond to experimental data for no penetration.

shown by the horizontal green dashed line in Fig. 2, in which the linear energy density of pore formation takes the value of $e = 20 k_B T$ [34]. If the deformation energy at steady state is smaller than pore formation energy ($\Delta E^* < 0$), the cell membrane will not be penetrated, as shown by Figs. 2(a) and 2(b) in which $\theta = 0$ and $\theta = 10^\circ$ ($r = 300$ nm). However, when the truncated nanocones have a large tilted angle [Figs. 2(c) and 2(d)], the deformation energy becomes greater than the pore formation energy, i.e., $\Delta E^* > 0$, which indicates the cell membrane corresponds to the penetration state. Similar results can also be found in Figs. 2(d)–2(h) when the radius of nanostructures is equal to 100 nm.

From Figs. 2(a)–2(d), we find that a larger tilted angle corresponding to the easier cell is to be penetrated when the radius is fixed. In the case $r = 300$ nm, the deformation energy of the membrane is determined mainly by the stretching energy and the bending energy can be ignored (see Appendix B). During the adhesion process, adhesion energy promotes cell adhesion, but stretching energy resists it. Adhesion energy is directly proportional to adhesion area, S_{ad} . Stretching energy is directly proportional to the square of change of cell area, ΔS^2 . Both S_{ad} and ΔS increase with cell adhesion. So, we can define a dimensionless parameter, i.e., adhesion area factor as $\Psi = S_{ad}/\Delta S$, to account for the competition between adhesion energy and stretching energy. The adhesion area

factor has the relation with tilted angle as $\Psi = 1/(1 - \sin \theta)$, meaning that a larger θ corresponds to a larger adhesion area factor. The larger adhesion area factor represents larger adhesion energy which can resist larger stretching energy. So, the cell membrane adhered to nanostructures with a large Ψ has an intensive deformation (large deformation energy) at steady state. In other words, the cell membrane is much more easily penetrated by the nanostructures with a larger θ (the detailed calculation method and discussions can be found in Appendix C).

From Figs. 2(e) and 2(f) we can get that the cell membrane can be penetrated when r becomes small to 100 nm. The main reason is the pore formation energy decreases with decreasing radius of nanostructures. However, the deformation energy at steady state is slightly affected by radius of nanostructures (see Appendix C). So, the cell membrane is much more easily penetrated by the nanostructures with a smaller r .

Based on the analysis above and using Eq. (7), we can calculate ΔE^* as a function of the radius and surface distribution density of the truncated nanocones, which allows us to construct a phase diagram to clarify the inter-related effects of the radius and surface distribution density on the cell penetration, as shown in Fig. 3. Obviously, we can divide the regions into two zones according to the value of ΔE^* , penetration region ($\Delta E^* > 0$) and no-penetration region

($\Delta E^* < 0$), which is demarcated by the white line representing $\Delta E^* = 0$.

Importantly, the dividing line, i.e., the relation of r and ρ when $\Delta E^* = 0$, can be obtained by simplifying our model. The bending energy of the cell membrane can be neglected when the radius of the nanostructure, r is large enough, as the discussion above (see Appendix B). So, the total free energy can be simplified to $E = -\gamma S_{ad} + E_{str}$. From $\partial E / \partial l = 0$, one can derive the critical adhesive depth at the stable state l^* . Substituting l^* into the simplified $\Delta E^* = E_{str}^* - 2\pi r e = 0$, we can obtain the crossover radius or crossover density that

$$r_c = \gamma^2 / [4\pi e \lambda \rho (1 - \sin \theta)^2], \quad (10)$$

or

$$\rho_c = \gamma^2 / [4\pi e \lambda r (1 - \sin \theta)^2]. \quad (11)$$

Equations (10) and (11) show the relation of crossover radius and crossover density, as shown by the red dotted line in Fig. 3. We can find that the red dotted line agrees well with the white line, which proves that it is reasonable to neglect the effects of bending energy in this case. Equations (10) and (11) are the key results of our model, which reveals the relationship of the penetration of the cell membrane with geometrical factors (radius, density, and tilted angle) of nanostructure and properties of the cell membrane (adhesion energy between membrane and the surface, stretching modulus, and linear energy density of pore formation). We can intuitively predict whether the cell membrane can be penetrated by various geometric of nanostructures according to Eqs. (10) and (11). We can find that it is more favorable for the cell membrane to be penetrated by the nanostructures with small radius or low density. The reason why the cell membrane is easily penetrated by small-radius nanostructures is that the penetration only needs formation of a pore with a small size, i.e., a small pore formation energy, as we discussed earlier. The adhesion depth is closely related to the density of the nanostructures, and the change of the area strongly depends on the adhesion depth. Therefore, the nanostructures density not only affects the original area (S_0), but also affects the depth of cell adhesion, i.e., the area change (ΔS). By combining Eq. (8) with Eq. (9), it can be concluded that the deformation energy of the cell membrane in a steady state is inversely proportional to the density, so the membrane has a high deformation energy at low density, which results in that it is easier to form pores. In short, the cell membrane has a larger deformation area under a low density than that under a high density. So, the deformation energy stored in the cell membrane is greater (see Appendix C for detailed discussion).

Besides, we can find from Fig. 3(a) that ΔE^* is also greater than zero when the radius is very small (about smaller than 6 nm). This is because the cell will be in the top state in this case due to the extremely large surface curvature of the nanostructure. The critical radius is equal to $r = \sqrt{\kappa / (2\gamma)}$, which has been discussed in detail in our previous work [30].

Besides the effects of the radius and surface distribution density, the height of nanostructures also influences the cell penetration. Taking vertical nanopillars ($\theta = 0$) as an example, if the height of nanopillars is smaller than the critical

adhesion depth, the cell membrane can completely wrap the nanopillars and adhere to the bottom of the substrate. In this case, the deformation energy will be smaller than that of the case of infinite nanopillars. Figures 4(a)–4(d) show the values of ΔE^* when the height is 5, 1, 0.5, and 0.15 μm , respectively. We find that the crossover white lines ($\Delta E^* = 0$) in Figs. 4(a)–4(c) are the same, which is because the height of nanopillars is much larger than the critical adhesion depth. However, when the height of nanopillars becomes very small, critical adhesion depth becomes larger than the height of nanopillars and the cell membrane can completely wrap the nanopillars. In this case, the deformation of the cell membrane cannot achieve the requirement for forming pore. So, there is no penetration when the height of nanopillars is very small, as shown in Fig. 4(d) in which $h = 0.15 \mu\text{m}$. A similar phenomenon is also found in Fig. 4(c), in which a no-penetration region appears when the radius and density are small. It is also because the cell has a larger critical adhesion depth than height of nanopillars and membrane completely wraps the nanopillars in this case.

In order to test our model, we did our best to collect experimental data that reported cell penetration by nanostructures in literature. Table I shows the comparison of experimental results and theoretical predictions for vertical nanopillars ($\theta = 0$), in which the first part (“Experimental data”) summarizes the experimental details of each case (cell type, nanopillars material, nanopillars size, and density) and whether the cell membrane is found to be penetrated. The last part (“Theoretical results”) lists the predicted crossover radius and predicted cell penetration states by the model using experimental parameters. If the radius in experiments is below the predicted crossover radius, the cell membrane should be found as penetration. On the contrary, the cell membrane should be found as no penetration if the radius in experiments is larger than the predicted crossover radius. The theoretical results successfully predict the penetration of the cell membrane of cases 1–3 and 6–8 in which nanopillars have a relatively small radius or low density. It also correctly predicts the no penetration in cases 4, 5, and 10, in which nanopillars have a relatively large radius or high density. These experimental data are also marked in Fig. 3(a). However, it can be found that the experimental data of cases 9 and 11 do not match our theoretical predictions. In spite of the disagreement, the experimental results just validate our model by combining the cases 8–11 which are all taken from the same literature. The study by VanDersarl *et al.* [19] is particularly interesting, because it is the only study where the effects of nanopillars radius and density on cell penetration were systematically investigated. They found that the cell corresponds to the penetration state when the nanopillar density or radius is small ($r = 50 \text{ nm}$, $\rho = 0.1 \mu\text{m}^{-2}$ or $r = 50 \text{ nm}$, $\rho = 1 \mu\text{m}^{-2}$), while there is no cell penetrations for large radius or high density ($r = 50 \text{ nm}$, $\rho = 10 \mu\text{m}^{-2}$ or $r = 375 \text{ nm}$, $\rho = 0.1 \mu\text{m}^{-2}$). The trends of effects of radius and density in this experiment are consistent with our conclusions which show that the nanostructures with small radius or low density correspond to cell penetration. Although our predicted crossover radius in cases 9 and 11 is inconsistent with the experimental data, the gap between them is small, which may be caused by the parameters used in our calculations (adhesion energy between membrane and the

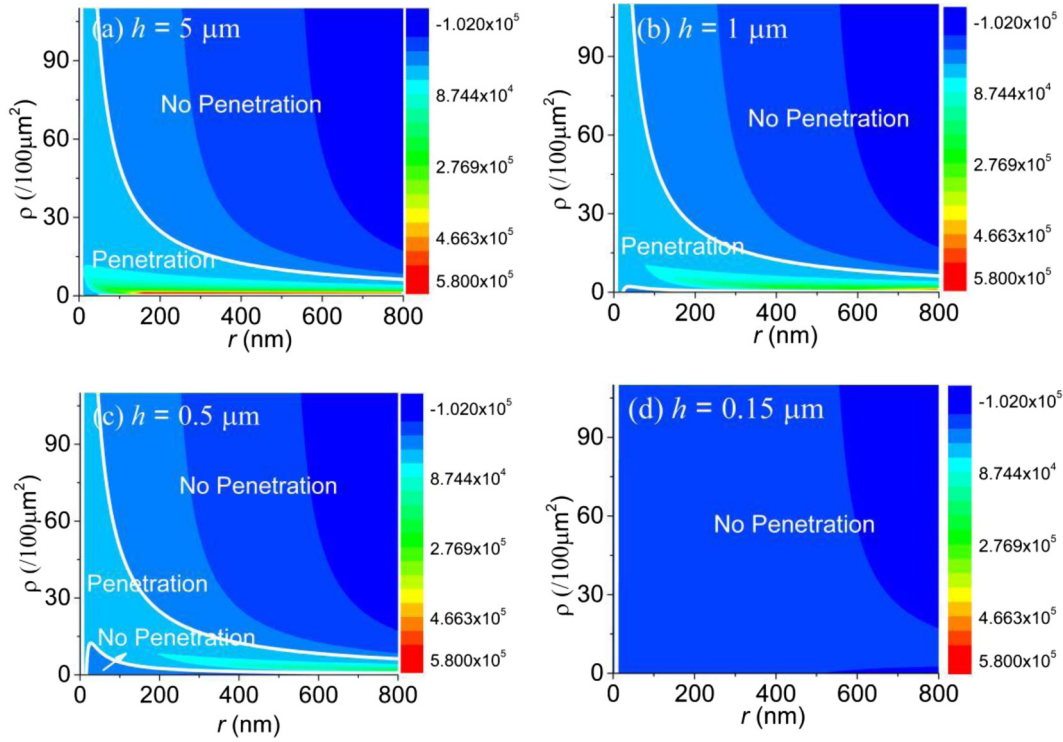


FIG. 4. The cell penetration diagram in the space of the $r - \rho$ plane for the vertical nanopillars ($\theta = 0^\circ$) with finite height of (a) $h = 5 \mu\text{m}$, (b) $h = 1 \mu\text{m}$, (c) $h = 0.5 \mu\text{m}$, and (d) $h = 0.15 \mu\text{m}$.

surface, stretching modulus, and linear energy density of pore formation).

Table II lists the effects of truncated nanocones on cell penetration. The model successfully predicts the penetration state of the cell membrane of cases 2–5 in which truncated nanocones have a relatively small radius or density. Conversely, the truncated nanocone with a relatively large radius or density represents no penetration of the cell membrane of cases 1 and 6. The experimental results show that the cell can be penetrated by the nanocones with small radius or small density, while the cell membrane cannot be penetrated when

radius or density is large. These experimental observations are consistent with our theoretical conclusions. Importantly, crossover radii predicted by our theory are in good agreement with the experiments.

Interestingly, when bacteria adhered on cicada-winglike nanopatterned surfaces, the bacterial membranes can be mechanically ruptured by nanostructures [35]. The related theoretical models have been found to study bactericidal mechanism of nanopatterned surfaces and suggest that the bacterial membrane can be mechanically ruptured when stretching degree of membrane exceeds the limit of bacterial

TABLE I. Summary of case studies from the literature where the observed mode of cell penetration can be compared with the predictions of the model for vertical nanopillar arrays. Case numbers correspond to references: 1 = Ref. [27], 2 = Ref. [20], 3 = Ref. [22], 4, 5 = Ref. [42], 6 = Ref. [21], 7 = Ref. [26], 8, 9, 10, 11 = Ref. [19].

Case	Cell type	Material	Experimental data				Theoretical results	
			$r(\text{nm})$	$h(\mu\text{m})$	Density (/100 μm^2)	Penetration	Crossover radius (nm)	Predicted penetration
1	CHO	Polyornithine-coated nanostraw	50	1	26-36	YES	191-138	YES
2	CHO	poly-D-lysine/fibronectin nanowire	50	1.5	30	YES	165	YES
3	CHO	Polycarbonate nanostraw	50	1	30	YES	165	YES
4	Cardiomyocytes	SiO ₂ nanopillar	100	1	100	NO	49.7	NO
5	Cardiomyocytes	SiO ₂ nanopillar	250	1	100	NO	49.7	NO
6	mES Cells	Silicon nanowires	45	6	20-30	YES	248-166	YES
7	C3H10T1/2	Silicon nanopillars	200	5	6.25	YES	796	YES
8	Hela/CHO	Al ₂ O ₃ nanostraws	50	1-2	10	YES	497	YES
9	Hela/CHO	Al ₂ O ₃ nanostraws	50	1-2	100	YES	49.7	NO
10	Hela/CHO	Al ₂ O ₃ nanostraws	50	1-2	1000	NO	4.97	NO
11	Hela/CHO	Al ₂ O ₃ nanostraws	375	1-2	10	NO	497	YES

TABLE II. Summary of case studies from the literature where the observed mode of cell penetration can be compared with the predictions of the model for truncated nanocone arrays where r represents tilted nanopillars' top radius, θ represents truncated nanocones' tilted angle, and h is tilted nanopillars' height. Case numbers correspond to references: 1, 2, 3 = Ref. [18], 4 = Ref. [29], 5, 6 = Ref. [25].

Case	Experimental data						Theoretical results		
	Cell type	Material	r (nm)	θ (°)	h (μ m)	Density (/100 μ m ²)	Penetration	Crossover radius (nm)	Predicted penetration
1	NIH-3T3	SU-8 nanopillar	45	1.15	1	177	NO	29.2	NO
2	NIH-3T3	SU-8 nanopillar	45	1.15	1	100	YES	51.7	YES
3	NIH-3T3	SU-8 nanopillar	45	1.15	1	25	YES	207	YES
4	CHO	Carbon nanofiber	10-25	4-3.88	7	4	YES	1436-1255	YES
5	FAO/Huh7	Silicon nanoneedle	50-150	3.68-2.86	7	4	YES	1418-1376	YES
6	FAO/Huh7	Silicon nanoneedle	150	2.86	7	40	NO	137	NO

Note: The angles θ in the list are calculated based on the bottom radius r_b of the truncated nanocone, the bottom radius is 65 nm in cases 1–3, 500 nm in cases 4–6. The calculation formula is $\theta = \arctan[(r_b - r)/h]$.

membrane [36–40]. However, the penetration mechanism of cell membrane introduced in this paper is different from the bactericidal mechanism of nanopatterned surfaces. The formation of a pore caused by cell membrane deformation requires an energy, i.e., pore formation energy. The deformation energy stored in the membrane exceeds the pore formation energy; the deformation energy can drive cell membrane pores formation, i.e., cell membrane to be penetrated. Specifically, the formation of cell membrane pore can effectively reduce the deformation energy stored in the membrane by reducing the membrane area and the bending deformation at the position of membrane pore. Because the top of the nanopillars has the maximum surface curvature (that is, the maximum bending energy), the deformation energy at the local region is larger than other regions. So, the pore forms easily at the position because the deformation energy can be reduced by the most. Therefore, we can judge cell membrane penetration by comparing the deformation energy and the pore formation energy.

Note that we assume that the cell membrane would wrap around the nanostructures intimately, following the contour of the nanostructures precisely. In particular, the nonadhesion cell membrane between nanostructures should be deformed. The energy change induced by the deformation of the nonadhesion cell membrane between nanostructures has been investigated and it is found that it is much smaller than the bending energy in other parts of cell membrane [39]. So, the bending energy of the cell membrane between the nanostructures contributes little to the total energy of the system. Therefore, in order to simplify our model and highlight the main influencing factors, we ignore the influence of the deformation of membrane between the nanostructures. The similar simplifications have also been widely used in the study of cell adhesion on patterned surface [28,30,36,37,41]. It should be noted that we also assume that the cell membrane is a thin elastic layer and neglect the thickness composition of the layer because the size of the nanostructures is much larger than the thickness of the cell membrane.

IV. CONCLUSIONS

In conclusion, through analyzing the free-energy change of cell adhered to the nanostructures surface, we have proposed

a cell penetration model which can predict whether the cell membrane can be penetrated by nanostructures. By comparing the deformation energy with the pore formation energy, we propose that the cell membrane can be penetrated by nanostructures if the deformation energy is greater than the pore formation energy. Otherwise, the cell membrane cannot be penetrated. Taking vertical nanopillars and truncated nanocones as examples, by calculating the difference between deformation energy and pore formation energy, we obtained a diagram of the cell penetration under the effects of the radius and distribution densities of nanostructures, which indicates that the cell can be penetrated by the nanocones or nanopillars with small radius or low density, while the cell membrane cannot be penetrated when radius or density is large. Furthermore, we provide a simple method to evaluate the crossover radius or density for the cell penetration. The results of the theory and the experiments have reached broad agreement, which implies that these studies would provide useful guidance to the design of nanopatterned surfaces for biomedical applications.

ACKNOWLEDGMENTS

This work was financially supported by National Natural Science Foundation of China (Grant No. 61875056), Science and Technology Program of Guangzhou (Grants No. 2019050001 and No. 201805010002), and Natural Science Foundation of Guangdong Province (Grant No. 2018A030313125).

APPENDIX A: DERIVATION OF THE CRITICAL ADHESIVE DEPTH

Considering the effects of the adhesion energy, bending energy, and stretching energy, the total free energy can be written as

$$E = - \int_{S_{ad}} \gamma dA + \int_{S_b} \left[\frac{\kappa}{2} (c_1 + c_2 - c_0)^2 \right] dS + \frac{1}{2} \lambda \frac{\Delta S^2}{S_0}, \quad (\text{A1})$$

where γ is the adhesion energy per unit area between the cell membrane and the surface; S_{ad} is the adhesion area between the cell and the surface. κ is the bending

modulus of the membrane, $c_1(c_2)$, c_0 denote the principal curvatures of the bending membrane surface and the spontaneous curvature, respectively, S_b is the intracellular bending area. λ denotes the stretching modulus of the membrane, ΔS and S_0 denote the intracellular area change by stretching and the cell area before stretching, respectively. The first term is adhesion energy, the second term

represents stretching energy, and the third term is bending energy.

The surface principal curvature of the truncated nanocones is $c_1 = 0$, and $c_2 = \cos \theta / (r + x \tan \theta)$, the cell membrane area in our selected period square domain before stretching, S_0 , is equal to $1/\rho$, and $\Delta S = \pi l(2r + l \tan \theta) / \cos \theta + \pi r^2 - \pi(r + l \tan \theta)^2$. Calculate the total energy as

$$E = - \int_0^l \gamma 2\pi(r + x \tan \theta) d\left(\frac{x}{\cos \theta}\right) + \int_0^l \frac{\kappa}{2} \left(\frac{\cos \theta}{r + x \tan \theta}\right)^2 2\pi(r + x \tan \theta) d\left(\frac{x}{\cos \theta}\right) + \frac{\lambda}{2} \frac{[\pi(2r + l \tan \theta) \frac{l}{\cos \theta} + \pi r^2 - \pi(r + l \tan \theta)^2]^2}{1/\rho}, \quad (\text{A2})$$

i.e.,

$$E = - \frac{\gamma \pi}{\cos \theta} l(2r + l \tan \theta) + \pi \kappa \frac{\cos^2 \theta}{\sin \theta} \ln \frac{r + l \tan \theta}{r} + \frac{\lambda}{2} \frac{[\pi(2r + l \tan \theta) \frac{l}{\cos \theta} + \pi r^2 - \pi(r + l \tan \theta)^2]^2}{1/\rho}. \quad (\text{A3})$$

Therefore, the equilibrium state of the system has a lowest free energy and we can obtain the minimum of free energy change through

$$\frac{\partial E}{\partial l} = 0, \quad (\text{A4})$$

i.e.,

$$- \frac{2\gamma \pi}{\cos \theta} (r + l \tan \theta) + \frac{\pi \kappa \cos \theta}{r + l \tan \theta} + 2\pi^2 \lambda \rho \times \tan \theta (1/\sin \theta - 1)^2 (r + l \tan \theta) [(r + l \tan \theta)^2 - r^2] = 0. \quad (\text{A5})$$

Solving Eq. (A5), we can obtain critical adhesive depth as

$$l^* = \sqrt{(\sqrt{b^2 - 4ac} - b)/2a - r} / \tan \theta, \quad (\text{A6})$$

where $a = 2\pi^2 \lambda \rho \tan \theta (1/\sin \theta - 1)^2$, $b = -(ar^2 + 2\gamma \pi / \cos \theta)$, $c = \pi \kappa \cos \theta$.

APPENDIX B: THE CONTRIBUTION OF BENDING ENERGY TO DEFORMATION

Figure 5 shows the calculated values of bending energy, stretching energy, and deformation energy in the space of the $r - \rho$ plane under infinite long nanopillars. The bending energy is determined by the bending energy density and bending area. When r is large, the curvature of cell membrane is very small, so the density of bending energy is very small. Moreover, the adhesion depth is also small in the case of large radius, which means that the adhesion area becomes small, which finally leads to the negligible bending energy, as shown in Fig. 5.

When radius r is small, the curvature of cell membrane increases and the bending energy per unit area increases. If the density of the nanostructure increases, the cell is at the tip of the nanostructure array, and the adhesion depth becomes very small, so the area decreases. So when radius r is small, and ρ is large, the bending energy is also very small, which

finally leads to the negligible bending energy. On the contrary, when the density of the nanostructure array is small in the case of small radius, the adhesion depth and the adhesion area increase, so the bending energy increases, and the contribution of the bending energy to the deformation energy becomes larger, which cannot be ignored. How the specific adhesion depth varies with the radius and density of the nanostructured array has been mentioned in our previous work [30]. In conclusion, the values of bending energy are much smaller than the stretching energy in the case of the nanopillars with large radius or high density, the bending energy cannot be ignored.

APPENDIX C: DERIVATION AND DISCUSSION OF ADHESION AREA FACTOR

As discussed in Appendix B, the deformation energy of membrane is determined mainly by the stretching energy, and the bending energy can be ignored when the nanostructure has not very small radius or low density. In this case, the total free energy can be written as $E = -\gamma S_{ad} + \frac{\lambda}{2} \frac{\Delta S^2}{S_0}$. During the adhesion process, adhesion energy promotes cell adhesion, but stretching energy resists it. Adhesion energy is directly proportional to adhesion area, S_{ad} . Stretching energy is directly proportional to the square of change of cell area, ΔS^2 . Both S_{ad} and ΔS increase accompanying with cell adhesion. So, we can define a dimensionless parameter, i.e., adhesion area factor that $\Psi = S_{ad} / \Delta S$. For truncated nanocones,

$$\Psi = \frac{\pi l(2r + l \tan \theta) / \cos \theta}{\pi l(2r + l \tan \theta) / \cos \theta + \pi r^2 - \pi(r + l \tan \theta)^2}, \quad (\text{C1})$$

i.e.,

$$\Psi = \frac{1}{1 - \sin \theta}. \quad (\text{C2})$$

According to Eq. (C2), adhesion area factor Ψ is determined by tilted angle θ and a larger tilted angle θ corresponds to a larger adhesion area factor. Besides, according to the

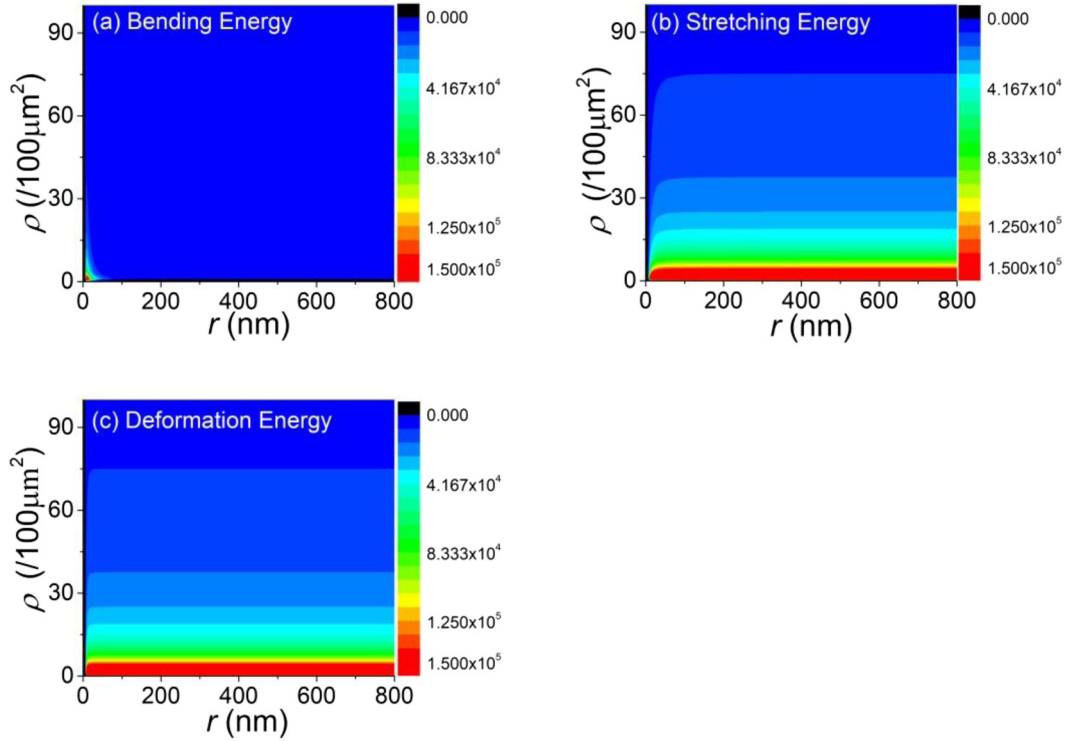


FIG. 5. The magnitudes of the energetic contributions associated with (a) bending energy, (b) stretching energy of the membrane, and (c) deformation energy have been plotted against truncated nanocones ($\theta = 0^\circ$) radius and distribution density.

definition of adhesion area factor, the total free energy also can be written as

$$E = -\gamma\Psi\Delta S + \frac{\lambda}{2} \frac{\Delta S^2}{S_0}. \tag{C3}$$

From $\partial E/\partial \Delta S = 0$, one can derive the critical change area of cell membrane at the stable state, which can be written as

$$\Delta S^* = \frac{\gamma\Psi}{\lambda\rho} \tag{C4}$$

And, the critical adhesion area of cell membrane at the stable state can be written as

$$S_{ad}^* = \Psi\Delta S^*, \tag{C5}$$

i.e.,

$$S_{ad}^* = \frac{\gamma\Psi^2}{\lambda\rho}. \tag{C6}$$

Adhesion energy and stretching energy are written as

$$E_{ad}^* = -\frac{\gamma^2\Psi^2}{\lambda\rho}, \tag{C7}$$

$$E_{str}^* = \frac{\gamma^2\Psi^2}{2\lambda\rho}. \tag{C8}$$

In Fig. 6(a), we calculate the adhesion energy, bending energy, stretching energy, and pore formation energy as a

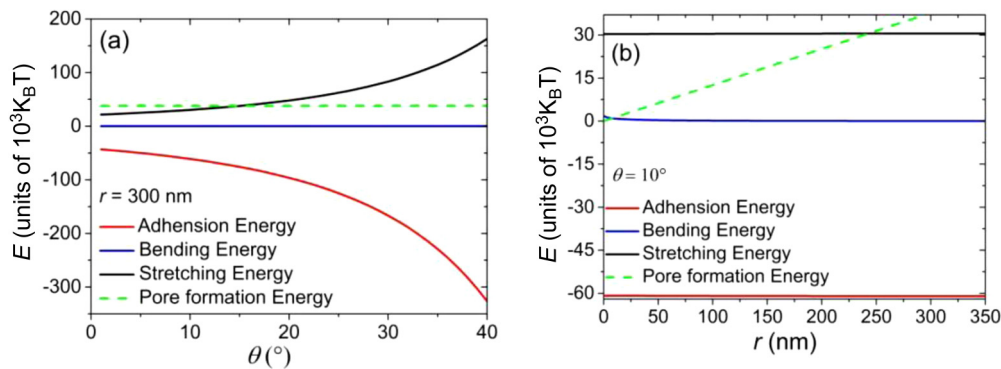


FIG. 6. (a) The calculated adhesion energy, bending energy, stretching energy, and pore formation energy as a function of tilted angle θ when surface distribution densities is $\rho = 0.3 \mu\text{m}^{-2}$, and the radius $r = 300 \text{ nm}$, respectively. (b) The calculated adhesion energy, bending energy, stretching energy, and pore formation energy as a function of radius r when surface distribution densities is $\rho = 0.3 \mu\text{m}^{-2}$, and tilted angle $\theta = 10^\circ$, respectively.

function of tilted angle θ . We find that a larger tilted angle θ corresponds to larger stretching energy and adhesion energy at steady state. So, cell membrane adhered to nanostructures with a large θ has an intensive deformation (large deformation energy) at steady state, and is easily penetrated by the nanostructures. This conclusion can also be obtained according to Eqs. (C4)–(C8). The larger adhesion area factor Ψ represents larger adhesion area and the change area of cell membrane which have larger adhesion energy and deformation energy, respectively.

We calculate the adhesion energy, bending energy, stretching energy, and pore formation energy as a function of radius r in Fig. 6(b). We can get that cell membrane can be

penetrated when r is small. The main reason is the pore formation energy decrease with decreasing radius of nanostructures. However, the deformation energy is slightly affected by radius of nanostructures at steady state. So, cell membrane is much more easily penetrated by the nanostructures with a smaller r .

According to Eqs. (C4) and (C6), we can know that both S_{ad} and ΔS are inversely proportional to nanostructures density, and the deformation energy stored in the cell membrane in the case of low density is greater than that in the case of high density. Therefore, it is more favorable for cell membrane to be penetrated by the nanostructures with low density.

-
- [1] J. Sekine, S. C. Luo, S. Wang, B. Zhu, H. R. Tseng, and H. H. Yu, *Adv. Mater.* **23**, 4788 (2011).
- [2] X. Liu, L. Chen, H. Liu, G. Yang, P. Zhang, D. Han, S. Wang, and L. Jiang, *NPG Asia Mater.* **5**, e63 (2013).
- [3] N. Sun, X. Li, Z. Wang, R. Zhang, J. Wang, K. Wang, and R. Pei, *ACS Appl. Mater. Interfaces* **8**, 12638 (2016).
- [4] S. Wang, H. Wang, J. Jiao, K. J. Chen, G. E. Owens, K. Kamei, J. Sun, D. J. Sherman, C. P. Behrenbruch, H. Wu, and H. R. Tseng, *Angew. Chem. Int. Ed. Engl.* **48**, 8970 (2009).
- [5] L. A. Dykman and N. G. Khlebtsov, *Chem. Rev.* **114**, 1258 (2014).
- [6] X. Li and D. Xing, *Appl. Phys. Lett.* **97**, 153704 (2010).
- [7] P. Sharma, J. B. Shin, B. C. Park, J. W. Lee, S. W. Byun, N. Y. Jang, Y. J. Kim, Y. Kim, Y. K. Kim, and N. H. Cho, *Nanoscale* **11**, 4591 (2019).
- [8] M. Essone Mezeme and C. Brosseau, *Phys. Rev. E* **87**, 012722 (2013).
- [9] H. Jeon, S. Koo, W. M. Reese, P. Loskill, C. P. Grigoropoulos, and K. E. Healy, *Nat. Mater.* **14**, 918 (2015).
- [10] J. Park, D. H. Kim, H. N. Kim, C. J. Wang, M. K. Kwak, E. Hur, K. Y. Suh, S. S. An, and A. Levchenko, *Nat. Mater.* **15**, 792 (2016).
- [11] H. Amin, M. Dipalo, F. De Angelis, and L. Berdondini, *ACS Appl. Mater. Interfaces* **10**, 15207 (2018).
- [12] R. Elnathan, M. Kwiat, F. Patolsky, and N. H. Voelcker, *Nano Today* **9**, 172 (2014).
- [13] X. Liu and S. Wang, *Chem. Soc. Rev.* **43**, 2385 (2014).
- [14] M. Kwak, L. Han, J. J. Chen, and R. Fan, *Small* **11**, 5600 (2015).
- [15] J. Pan, Z. Lyu, W. Jiang, H. Wang, Q. Liu, M. Tan, L. Yuan, and H. Chen, *ACS Appl. Mater. Interfaces* **6**, 14391 (2014).
- [16] B. G. Nair, K. Hagiwara, M. Ueda, H. H. Yu, H. R. Tseng, and Y. Ito, *ACS Appl. Mater. Interfaces* **8**, 18693 (2016).
- [17] R. Elnathan, B. Delalat, D. Brodoceanu, H. Alhמוד, F. J. Harding, K. Buehler, A. Nelson, L. Isa, T. Kraus, and N. H. Voelcker, *Adv. Funct. Mater.* **25**, 7215 (2015).
- [18] K. S. Beckwith, S. Ullmann, J. Vinje, and P. Sikorski, *Small* **15**, 1902514 (2019).
- [19] J. J. VanDersarl, A. M. Xu, and N. A. Melosh, *Nano Lett.* **12**, 3881 (2011).
- [20] X. Xie, A. Aalipour, S. V. Gupta, and N. A. Melosh, *ACS Nano* **9**, 11667 (2015).
- [21] W. Kim, J. K. Ng, M. E. Kunitake, B. R. Conklin, and P. Yang, *J. Am. Chem. Soc.* **129**, 7228 (2007).
- [22] A. Aalipour, A. M. Xu, S. Leal-Ortiz, C. C. Garner, and N. A. Melosh, *Langmuir* **30**, 12362 (2014).
- [23] R. Ning, S. Wang, J. Wu, F. Wang, and J. M. Lin, *Small* **10**, 4113 (2014).
- [24] S. G. Higgins, M. Becce, A. Belessiotis-Richards, H. Seong, J. Sero, and M. M. Stevens, *Adv. Mater.* **32**, 1903862 (2020).
- [25] M. Denoual, M. Chiral, and B. Lepioufle, *J. Nanobiotechnology* **1**, 389 (2005).
- [26] M. A. Bucaro, Y. Vasquez, B. Hatton, and J. Aizenberg, *ACS Nano* **6**, 6222 (2012).
- [27] A. M. Xu, A. Aalipour, S. Lealortiz, A. H. Mekhdjian, X. Xie, A. R. Dunn, C. C. Garner, and N. A. Melosh, *Nat. Commun.* **5**, 3613 (2014).
- [28] H. Zang and X. Li, *Phys. Rev. E* **101**, 032406 (2020).
- [29] T. E. Mcknight, A. V. Melechko, G. D. Griffin, M. A. Guillorn, V. I. Merkulov, F. Serna, D. K. Hensley, M. J. Doktycz, D. H. Lowndes, and M. L. Simpson, *Nanotechnology* **14**, 551 (2003).
- [30] J. Zhou, X. Zhang, J. Sun, Z. Dang, J. Li, X. Li, and T. Chen, *Phys. Chem. Chem. Phys.* **20**, 22946 (2018).
- [31] S. Mirigian and M. Muthukumar, *J. Chem. Phys.* **139**, 044908 (2013).
- [32] Y. Sun, T. L. Sun, and H. W. Huang, *Biophys. J.* **107**, 2082 (2014).
- [33] D. Marsh, *Chem. Phys. Lipids* **144**, 146 (2006).
- [34] S. Pogodin and V. A. Baulin, *ACS Nano* **4**, 5293 (2010).
- [35] E. P. Ivanova, J. Hasan, H. K. Webb, V. K. Truong, G. S. Watson, J. A. Watson, V. A. Baulin, S. Pogodin, J. Y. Wang, and M. J. Tobin, *Small* **8**, 2489 (2012).
- [36] X. Li, *Phys. Chem. Chem. Phys.* **18**, 1311 (2016).
- [37] S. Pogodin, J. Hasan, V. A. Baulin, H. K. Webb, V. K. Truong, T. H. Phong Nguyen, V. Boshkovikj, C. J. Fluke, G. S. Watson, J. A. Watson, R. J. Crawford, and E. P. Ivanova, *Biophys. J.* **104**, 835 (2013).
- [38] K. Xiao, X. Cao, X. Chen, H. Hu, and C. Wu, *J. Appl. Phys.* **128**, 064701 (2020).
- [39] X. Li and T. Chen, *Phys. Rev. E* **93**, 052419 (2016).
- [40] G. S. Watson, D. W. Green, J. A. Watson, Z. Zhou, X. Li, G. S. P. Cheung, and M. Gellender, *Adv. Mater. Interface* **6**, 1801646 (2019).
- [41] N. Buch-Manson, S. Bonde, J. Bolinsson, T. Berthing, J. Nygard, and K. L. Martinez, *Adv. Funct. Mater.* **25**, 3246 (2015).
- [42] L. Hanson, Z. C. Lin, C. Xie, Y. Cui, and B. Cui, *Nano Lett.* **12**, 5815 (2012).